

**The development of a micro-mechanical apparatus applying combined normal-shear-bending forces to natural sand grains with artificial bonds**

Wanying Wang<sup>1</sup>, Matthew R. Coop<sup>2</sup> and Kostas Senetakis<sup>3\*</sup>

<sup>1</sup> Guangdong University of Technology, China, formerly City University of Hong Kong, Hong Kong SAR China

<sup>2</sup> UCL London UK

<sup>3</sup> City University of Hong Kong, Hong Kong SAR China

\* Corresponding author: [ksenetak@cityu.edu.hk](mailto:ksenetak@cityu.edu.hk)

**Full mail addresses of all authors:**

<sup>1</sup> Guangdong University of Technology (Civil Engineering), Guangzhou University City Outer Ring Road No. 100 (510006),  
Guangzhou, Panyu, China.

<sup>2</sup> Department of Civil, Environmental and Geomatic Engineering,  
University College London, Gower Street, London, WC1E 6BT, UK.

<sup>3</sup> Department of Architecture and Civil Engineering,  
City University of Hong Kong, (Academic Building 1, Blue Zone 6/F)  
Kowloon Tong, Kowloon, Hong Kong.

## **Abstract**

Natural soils are often cemented and there has been a need to understand better and properly model their behavior for the safe design and assessment of critical infrastructure. This necessitates the study of cemented soils at the scale of the grain. In this study, a new generation apparatus is presented which is capable of conducting complex load path tests on two natural sand grains cemented with an artificial bonding component. Thus the apparatus gives the opportunity to obtain insights into the micromechanics of cemented soils/weak rocks and contribute to the development of more accurate models to be utilized in the discrete element analysis of geo-materials. Apart from the presentation of the major technical features of the new apparatus, a description of the methods which were used for sample preparation and mounting as well as a preliminary set of experiments are presented and discussed in this note.

**Keywords:** micromechanics; cemented sand; complex load paths; laboratory tests

## **Introduction**

Over recent years, significant effort has been made by the research community to understand the mechanical behavior of granular materials using the Discrete Element Method (DEM) (Cundall and Strack, 1979). DEM studies have focused particularly on uncemented sands, but there have also been notable works on the simulation of cemented soils and rocks (Cundall, 1987; Potyondy and Cundall, 2004; O’Sullivan, 2011; Jiang et al. 2007; 2011; Cheung et al., 2013; De Bono and McDowell, 2014; Shen et al. 2016). Cementation between the particles occurs often in natural sands and results from depositional and diagenetic processes. A significant portion of engineering activities may involve bonded geo-materials, for example, lightly or moderately cemented soils as well as sedimentary rocks and there have been many attempts to examine these geo-materials in the laboratory through multi-scale studies and element-type tests with microscopic observations (e.g. Cuccovillo and Coop, 1999, Alvarado et al., 2012).

In DEM simulations of cemented geo-materials, an important input is the contact model for bonded grains (e.g. Jiang et al. 2006; Jiang et al. 2012b), the validation of which would typically require complex load path tests including normal and shear forces and moments. However, over recent years, there has been only limited work concerning the micromechanics of bonded grains (Jiang et al. 2012a; Jiang et al. 2015).

This note describes the basic technical features of a new micromechanical apparatus

which is capable of conducting experiments on cemented grains with the application of complex load paths, which allows a more systematic study into cemented sands at the grain scale. Preliminary results on Leighton Buzzard sand quartz grains cemented with gypsum are presented and discussed. The role of such an apparatus would be to provide the micro-mechanical input parameters needed for better DEM modeling of cemented sands.

### **New micromechanical apparatus**

#### *Basic technical features and loading paths*

A schematic illustration of the tests possible in the new apparatus is presented in Figure 1. Figure 1(a) shows a compression test simply using one loading device in the vertical direction. In Figure 1(b), the cemented particle is held by a pair of compressive forces in the vertical direction while another pair of horizontal forces is applied through the centreline of the sample, thus the sample is under combined compression and shearing. When the horizontal force is not along the centreline of the specimen, with an eccentric distance  $e_0$ , the sample is under compression, shearing and also a bending moment, as shown in Figure 1(c).

The loading apparatus (Figures 2 and 3), consists of a supporting frame, loading devices, loading mounts, load cells of a capacity of 1,000 N (sensitivity of 2mV/V and accuracy of 0.15%), Linearly Variable Differential Transformers (LVDTs) of high resolution and a microscope camera. Two linear actuators were used to load the cemented particle pair in orthogonal directions. The vertical stepper motor is fixed on

a disc and supported by three stainless-steel columns which are fastened to the base. The nuts on the columns are used to adjust the location of the circular plate and to make it level. The horizontal motor is assembled on a stainless-steel plate connected to the base. The experiments are controlled by a custom-built code developed for the apparatus. With the computer control, any load path with changing normal and shear loads can be followed. Since the eccentricity is fixed for each test, the apparatus may only follow paths with a constant ratio of shear force to bending moment. The apparatus can also perform either force or displacement control for both normal and shear.

In this study, the shear force was applied by the horizontal linear actuator with a speed of 0.2 mm/hr and the constant normal force was applied and controlled by means of the vertical linear actuator in a force-controlled manner. This speed was chosen so as to give tests of reasonable duration while ensuring accurate feedback control of the desired forces and/or displacements via the motors. Speeds of up to 0.5mm/hour are easily achievable by the apparatus and there is no lower limit to the speed because of the use of a feedback control. This speed of 0.2mm/hour also meant that videos capturing the sample response did not utilize excessive storage space, while being slow enough to make clear observations.

Four LVDTs were used in this apparatus. Two LVDTs were fixed on the base by a frame symmetrically above and below the horizontal loading end. The frame has a hole between these two LVDTs, allowing the loading end to move freely through it.

During the test, the armatures of these two LVDTs were glued on the surface of the L-shaped mount (Figure 3). The second pair of LVDTs was assembled about the vertical loading axis. To avoid the compliance of the vertical load cell or the connections above the upper mount affecting the accuracy of the displacement measurement, the two transducers were fixed on the upper mount, which is below the vertical load cell. The two transducers were assembled at the back of the upper mounts, so that the digital microscope camera can have a front view of the sample. For both the horizontal LVDTs and the vertical LVDTs, the displacements along each direction were calculated as the average value from the two LVDTs' readings and the rotation angle was calculated from the difference between the two readings. All the LVDTs have a resolution equal to 0.1 microns with a sensitivity of 375mV/V and an accuracy of 0.25%.

#### *L-shaped mounts*

The mounts to hold the cemented particles were designed to perform the three types of loading paths using one apparatus, without the necessity of major modifications between the different types of experiments. To allow the bond to be sheared, both the upper and lower mounts should be free to move along the travel direction of the stepper motor. Both mounts were designed as L shapes (Figure 3). The arms of the mounts enabled the external horizontal force to be applied at different heights. The left side, which is driven by the horizontal motor, was in contact with the upper mount arm to apply a horizontal force and the right side is the reaction end. Both of these

ends have sharp edges so the force is delivered at a single location in a plane perpendicular to the axis of the cemented particle, that is shearing. The L-shaped mounts are greased to reduce friction. The lower L-shaped mount and the reaction end could be moved vertically, which is achieved by two small lifting platforms under them, respectively. A calibrated screw is used to lift the platform up and down precisely. Since the loading arm at the left hand side is fixed on the support, by changing the height of the cemented particle and the reaction arm, a change of the eccentric distance  $e_0$  can be achieved (Figure 1(c) and Figure 3), thus a bending moment can be applied symmetrically about the horizontal centreline of the sample. It is noted that the Z-shaped reaction end is short and thick to increase the stiffness of the system during shearing and bending tests.

During the tests, the cemented particles are glued in the apparatus at both ends using epoxy resin. The two mounts are connected with the upper and lower parts by pins which allow the mounts to rotate freely under the bending tests. An optical microscope camera with a resolution of 640×480 pixels is placed in front of the sample for recording the tests. The microscope camera has an adjustable magnification up to 250x, but 50x was chosen in this study. The frame rate of the recording video is 30 fps.

### **Materials used and sample preparation**

For the set of preliminary experiments in the study, Leighton Buzzard sand (LBS) particles of the fraction 2.36-5.00 mm were used, which is a silica sand from the UK.

For the bonding component, gypsum plaster (Crystacal D from the UK) was used to cement pairs of the LBS grains. According to Wang et al. (2017), using gypsum plaster as the cementation material provides more consistent results for loading tests compared to Portland cement in terms of the compressive load – displacement relationship. Based on the previous data in Wang et al. (2017), the bonded LBS grains with gypsum would exhibit a compressive strength varying from about 300 to 480 N.

Artificially cemented particles were made using a pair of novel moulds made of perspex. After waiting for at least 24 hours for hardening of the bonding agent, the moulds were removed. A representative image of artificially cemented particle is shown in Figure 3. The bond thickness of the cemented particles used in this study is 2mm, which is “thick bond” as defined by Jiang et al. (2012a). This type of bonded grains prepared in the present study could represent, perhaps, lightly cemented sands and younger clastic rocks, rather than massive rocks of greater geological age or non-clastic type of rocks.

### **Frictional tests of the apparatus**

During the shear and combined shear-bending (called “bending”) tests, a constant value of vertical compression force is applied to the sample. The shear force acts on the L-shaped mount, so the frictional force between the tip of the horizontal loading end and the L-shaped mount where the horizontal force is applied should be investigated while the mount is moving vertically. Before the test, lubricating oil applied to the contact surface to minimize the friction. 10 N of horizontal force was

applied to the L shaped mount, which was then moved vertically driven by the vertical stepping motor with no sample in contact. The relationship between the vertical load and the displacement for a representative test is plotted in Figure 4. Due to the small friction in the apparatus, the vertical force becomes positive when the vertical motor moves upward and negative when it moves downward. It is noted that this friction is proportional to the applied horizontal load, and is about  $\pm 1.5$  N on average for 10 N of horizontal force.

## **Preliminary results**

### *Shearing and shearing-bending tests*

Figure 5 illustrates a representative shear force-horizontal displacement curve along with particle images for a compression, shear and bending combined test. In this loading path, a target normal force equal to 50 N, was applied first and then set as a constant. Then the vertical positions of the horizontal loading end and reaction arm were adjusted, making them symmetrical about the centre line of the cementation. For this test, the eccentricity of the shear force to the centre line was equal to 1.6mm.

In the bending tests, the horizontal displacements consist of two parts: one part resulting from the rotation of the upper mount, the other resulting from the shearing. Since the two horizontal LVDTs of the apparatus are placed symmetrical to the horizontal loading ends (Figures 2 and 4), the average value of the readings obtained from the two LVDTs is the shear displacement. The relationship between the shear force and shear displacement for a combined bending test is shown in Figure 5. With

the increase of the horizontal displacement, the increase of shear force becomes markedly slower. Finally, after a hardening regime, the shear force approaches a constant value of 35 N. In their study, Jiang et al. (2012a) noticed a softening regime for thick bonds, which was not the case for the data in Figure 5. The ratio of the peak shear force over the normal load is about 0.7 for this experiment. Due to the variety of the failure mechanisms affected by the morphology of the particles (Wang et al. 2017), it is very difficult to obtain a unique force-displacement or moment-rotation angle curve for one loading path. A very large number of tests should therefore be conducted to investigate thoroughly all the breakage mechanisms and modes of failure producing a realistic model for bonded grains under complex loading patterns, which is ongoing work by the authors.

The initial shear force was then applied to seat the sample firmly against the loading and reaction arms. At point 1 in Figure 5, the particle image shows no visible crack in the bond. At point 2, a barely visible inclined crack initiates at the bottom left, which is followed by crack propagation with the increase of shear force at point 3 and point 4. In this case, the bond breaks because the shear stress exceeds a critical value, even though global breakage of the bond, as for example happened in compressive tests (Wang et al. 2017), did not occur under the combined normal-shear-bending forces. It should be pointed out that the camera could only give a 2-dimensional image of the cemented particles behavior and that the crack propagation inside the specimen could not be observed. High-resolution X-ray CT might be a powerful tool to detect the internal structure of the specimens (Zhao et al., 2015), which was out of the scope of

the present study.

Figure 6 gives a representative shear force-horizontal displacement curve along with particle images for a pure shearing test under a normal load of 50 N (no application of bending moment in this case). The force-displacement relationship seems to be quite similar to the data in Figure 5. In the case of pure shearing, it was harder to observe the crack initiation and propagation through the test, which was clearer in Figure 5 with combined normal-shear-bending loading. At point 1, although the slope of the force-displacement curve changed, no obvious change could be observed in the video, possibly due to the lack of the spatial resolution of the camera. After reaching a peak value at point 2, the trend of the force-displacement curve changed to decreasing, while it could be found that the cemented particles rotated with no crack on the surface of the bond. This indicates that a possible separation between the grains and the bond occurred. It would be expected that for pure shearing, the ratio of the shear force to the normal force would be greater than that for a combined normal-shear-bending test. The results of Figure 6 showed a slightly lower value of the ratio shear force/normal force in comparison to Figure 5. This can be attributed to the scatter of the data due to the gypsum bonding from one test to another since for each new plot, a new pair of grains was used, and as Wang et al. (2017) showed in compression, the morphology of the sand grain – cement interface strongly affects the data.

*Shear force – displacement and bending moment - displacement relationships for*

### *representative tests*

Figure 7(a) illustrates the mechanical response for combined bending tests under the same constant normal force of 50 N in terms of shear force - horizontal displacement relationships. For these five tests, the eccentricity of the shear force to the centre line was again equal to 1.6 mm. The curves show the high stiffness of the cemented samples under compression, shearing and bending. The peak shear force of the cemented particles with a normal load of 50 N ranges from 24 N to 35 N while the displacement at failure varies from 0.06 mm to 0.18 mm. Again the data are quite inconsistent, probably because of the variable grain – cement morphology. The relationships between the bending moment and the rotation angle for the combined bending tests under a normal force of 50 N are given in Figure 7(b) for these five tests, and are highly non-linear.

### **Conclusions**

A new micromechanical apparatus has been developed, which is capable of testing cemented grains, using real soil particles and artificial bonds applying combined normal-shear-bending to the sample. This pattern of load and sample type allows obtaining insight into the micromechanical behavior of cemented soils or weak sandstones. The apparatus utilizes two systems each consisting of stepper motors, LVDTs and load cells. One system works in the horizontal direction applying shearing to the cemented grains and the second system works in the vertical direction, supported by a frame, applying the normal load to the sample. In the study, LBS

grains were used and the cementing component was gypsum which was also investigated in a previous study of compressive strength of cemented LBS grains (Wang et al. 2017). For the limited number of experiments in the study, the shear force – displacement relationship exhibited an increase with decreasing rate and after a hardening regime, plasticity dominated the response of the sample with an almost constant shear force under increasing displacement, without notable occurrence of a softening regime. The scatter of the data, similar to that of Wang et al. (2017), highlights the difficulties of obtaining repeatability with natural sand grains. The results are promising for future studies in the investigation and modeling of the micromechanics of cemented grains with major applications in soil and rock mechanics and there is an ongoing work by the authors in this direction.

### **Acknowledgements**

The study was fully supported by a grant from the Research Grants Council of the Hong Kong Special Administrative Region, China: Theme-based research project Scheme “Understanding Debris Flow Mechanisms and Mitigating Risks for a Sustainable Hong Kong” - Project No. T22-603/15 N (CityU 8779012).

### **References**

- Alvarado, G., Coop, M.R. and Willson, S. (2012) On the role of bond breakage due to unloading in the behaviour of weak sandstones. *Géotechnique* **62** (4), 303-316.
- Cheung L.Y.G., O’Sullivan C. and Coop M.R. (2013). Discrete Element Method simulations of analogue reservoir sandstones, *International Journal of Rock Mechanics and Mining Sciences* **63**, 93-103.
- Cuccovillo T. and Coop M.R. (1999). On the mechanics of structured sands, *Géotechnique*

**49**(6), 741-760.

Cundall P.A. (1987). Distinct element models of rock and soil structure. In: Brown ET, editor. *Analytical and computational methods in engineering rock mechanics*. London: Allen and Unwin. p. 129-63.

Cundall P.A., Strack O.D.L. (1979). A discrete numerical model for granular assemblies. *Géotechnique* **29**, 49-65.

De Bono J.P. and McDowell G.R. (2014). Discrete element modelling of one-dimensional compression of cemented sand. *Granular Matter* **16**(1), 79-90.

Jiang M. J., Yu H. S., Harris D. (2006). Bond rolling resistance and its effect on yielding of bonded granulates by DEM analyses. *International Journal for Numerical and Analytical Methods in Geomechanics* **30**, 723-761

Jiang M.J., Yu H.S., Leroueil S. (2007). A simple and efficient approach to capturing bonding effect in natural sands by discrete element method. *International Journal of Numerical Methods in Engineering* **69**(6), 1158-1193.

Jiang M.J., Yan H.B. Zhu, H.H. Utili, S. (2011). Modelling shear behavior and strain localization in cemented sands by two-dimensional distinct element method analyses. *Computer and Geotechnics* **38**(1), 14-29.

Jiang, M. J., Sun, Y. G., Li, L. Q., and Zhu, H. H. (2012a) Contact behavior of idealized granules bonded in two different interparticle distances: An experimental investigation. *Mechanics of Materials* **55**, 1-15.

Jiang M. J., Murakami A. (2012b). Distinct element method analyses of idealized bonded-granulate cut slope. *Granular Matter* **14**, 393-410.

Jiang, M. J., Jin, S. L., Shen, Z. F., Liu, W. and Coop, M. R. (2015) Preliminary experimental study on three-dimensional contact behavior of bonded granules. *International Symposium on Geohazards and Geomechanics (ISGG2015)* doi:10.1088/1755-1315/26/1/012007.

O'Sullivan C. (2011). Particulate discrete element modelling: A geomechanics perspective. *Applied Geotechnics* (vol. 4). Spon Press.

Potyondy D.O. and Cundall P.A. (2004). A bonded-particle model for rock. *International Journal of Rock Mechanics and Mining Sciences* **41**(8), 1329-1364.

Shen, Z., Jiang, M. and Thornton, C. (2016) DEM simulation of bonded granular material. Part I: Contact model and application to cemented sand. *Computers and Geotechnics* **75** 192-209.

Wang W., Nardelli V. and Coop M.R. (2017). The micro-mechanical behaviour of artificially cemented sand particles under compression and shear. *Geotechnique Letters* **7**, 1-7, <http://dx.doi.org/10.1680/jgele.16.00166>.

Zhao, B., Wang, J., Coop, M. R., Viggiani, G. & Jiang, M. (2015). "An investigation

of single sand particle fracture using x-ray micro-tomography”, *Geotechnique*. 65(8), 625-641.

## **LIST OF FIGURES**

**Figure 1** Schematic illustration of the different loading tests: (a) compression test; (b) combined compression-shear test; (c) combined compression, shear and bending test.

**Figure 2** New micromechanical apparatus for complex loading tests on cemented particle (Note: Frame width is equal to 110 mm).

**Figure 3** The mounts and connections of the apparatus and cemented particles with a thickness of 2 mm (Note: Frame width is equal to 110 mm).

**Figure 4** Results of frictional test

**Figure 5** Relationship between the shear force and horizontal displacement for a bending test (normal-shear-bending loading) under a normal force of 50N with microscope images of bond crack initiation and propagation

**Figure 6** Relationship between the shear force and horizontal displacement for a test with no bending (pure shearing) under a normal force of 50N with microscope images of bond crack initiation and propagation (Note that there was not observed very clearly crack initiation for this test)

**Figure 7** Mechanical response for the bending tests on GPLBS under a normal force of 50N (a) shear force-horizontal displacement (b) bending moment-rotation angle.

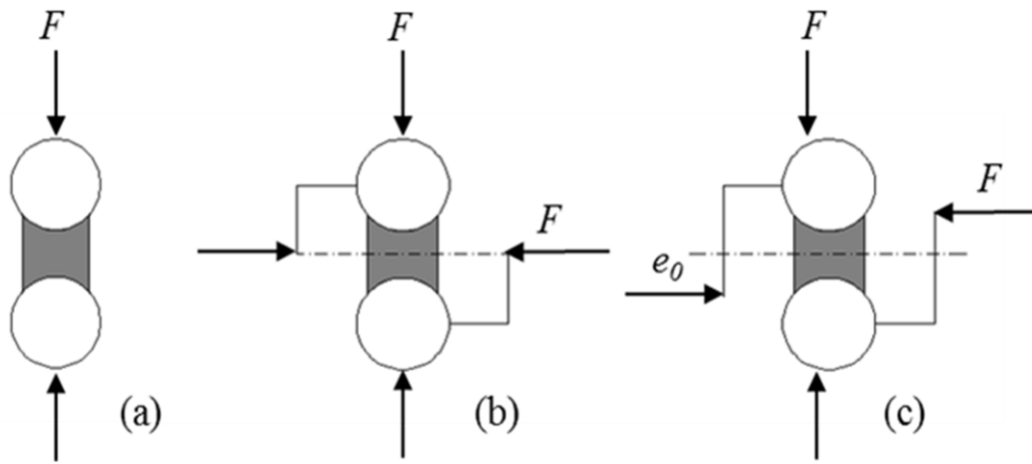


**Figure 1** Schematic illustration of the different loading tests: (a) compression test; (b) combined compression-shear test; (c) combined compression, shear and bending test.

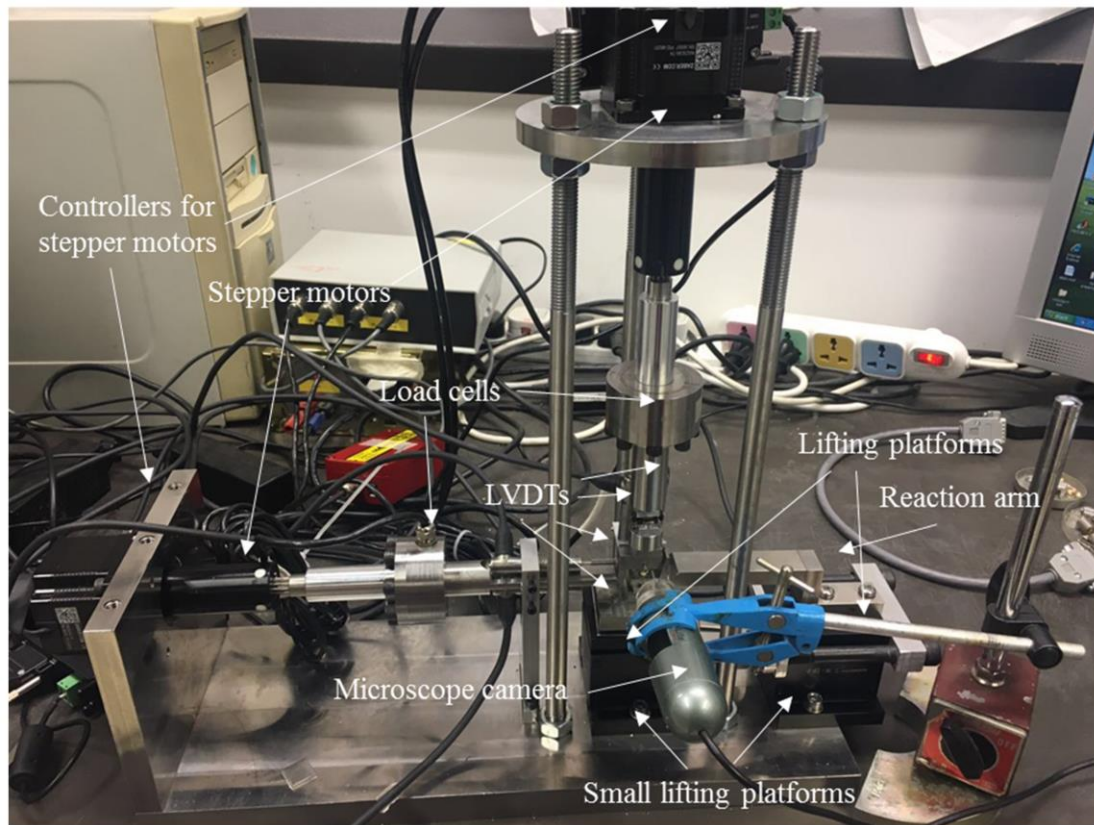


**Figure 2** New micromechanical apparatus for complex loading tests on cemented particle (Note: Frame width is equal to 110 mm).

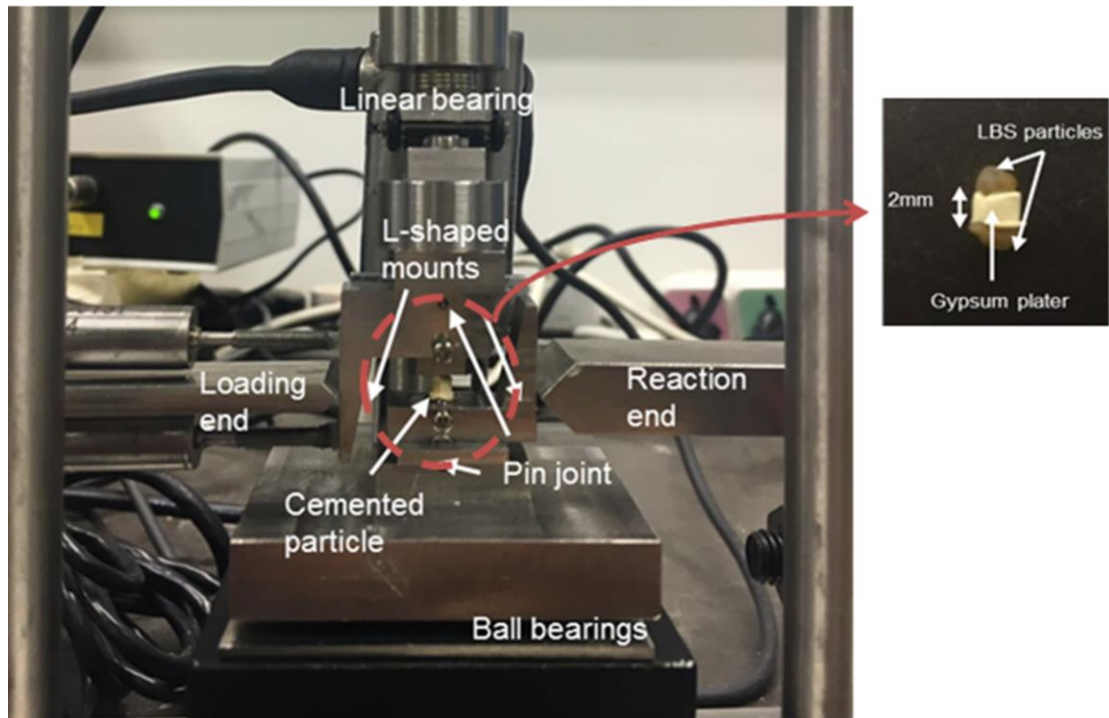


**Figure 3** The mounts and connections of the apparatus and cemented particles with a thickness of 2 mm (Note: Frame width is equal to 110 mm).

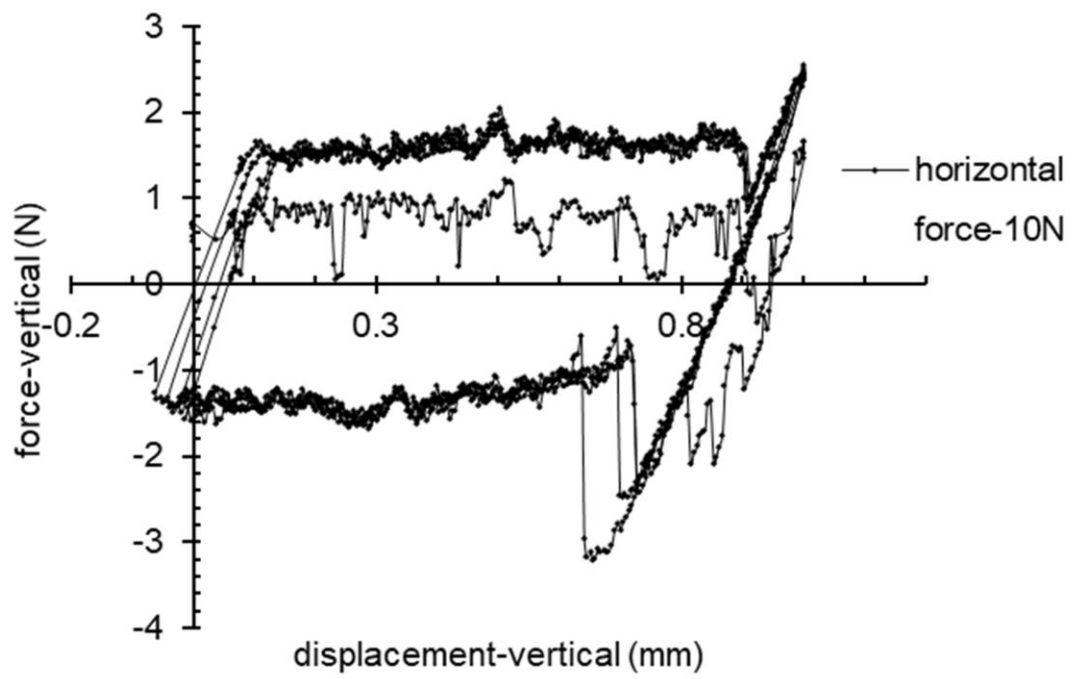


**Figure 4** Results of frictional test

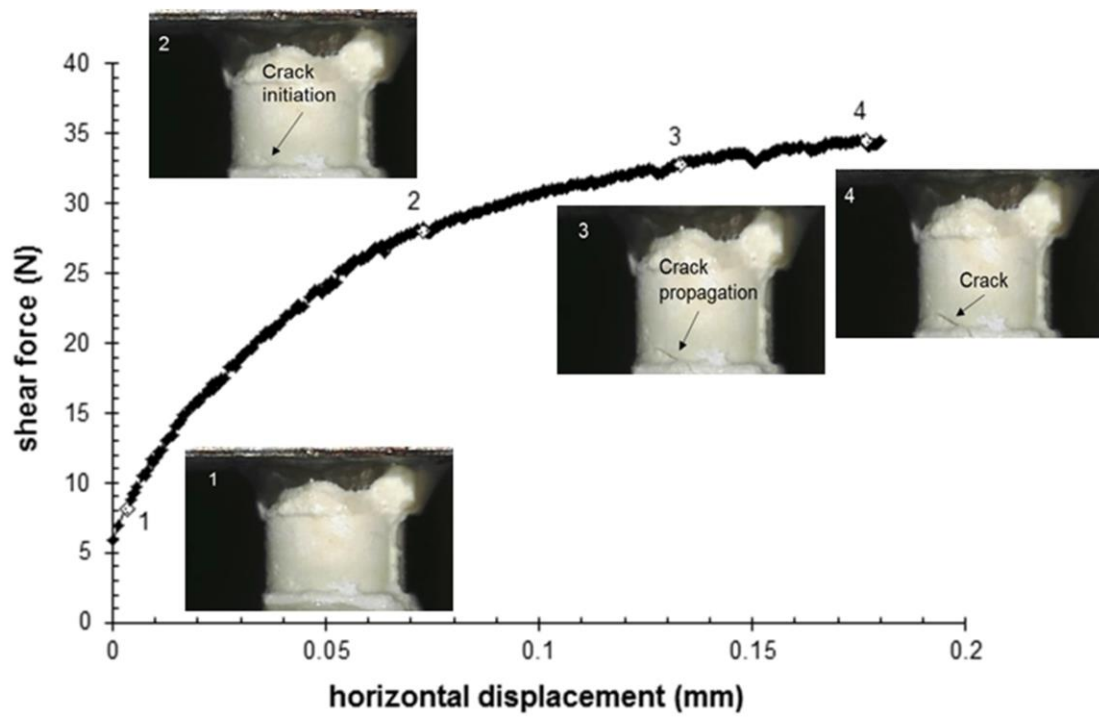


**Figure 5** Relationship between the shear force and horizontal displacement for a bending test (normal-shear-bending loading) under a normal force of 50N with microscope images of bond crack initiation and propagation

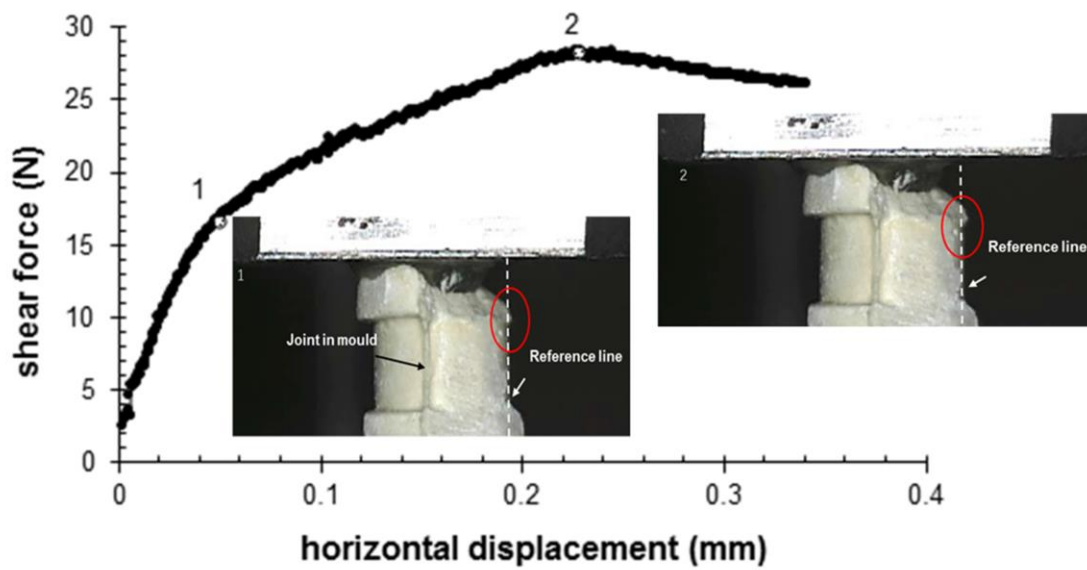


**Figure 6** Relationship between the shear force and horizontal displacement for a test with no bending (pure shearing) under a normal force of 50N with microscope images of bond crack initiation and propagation (Note that there was not observed very clearly crack initiation for this test)

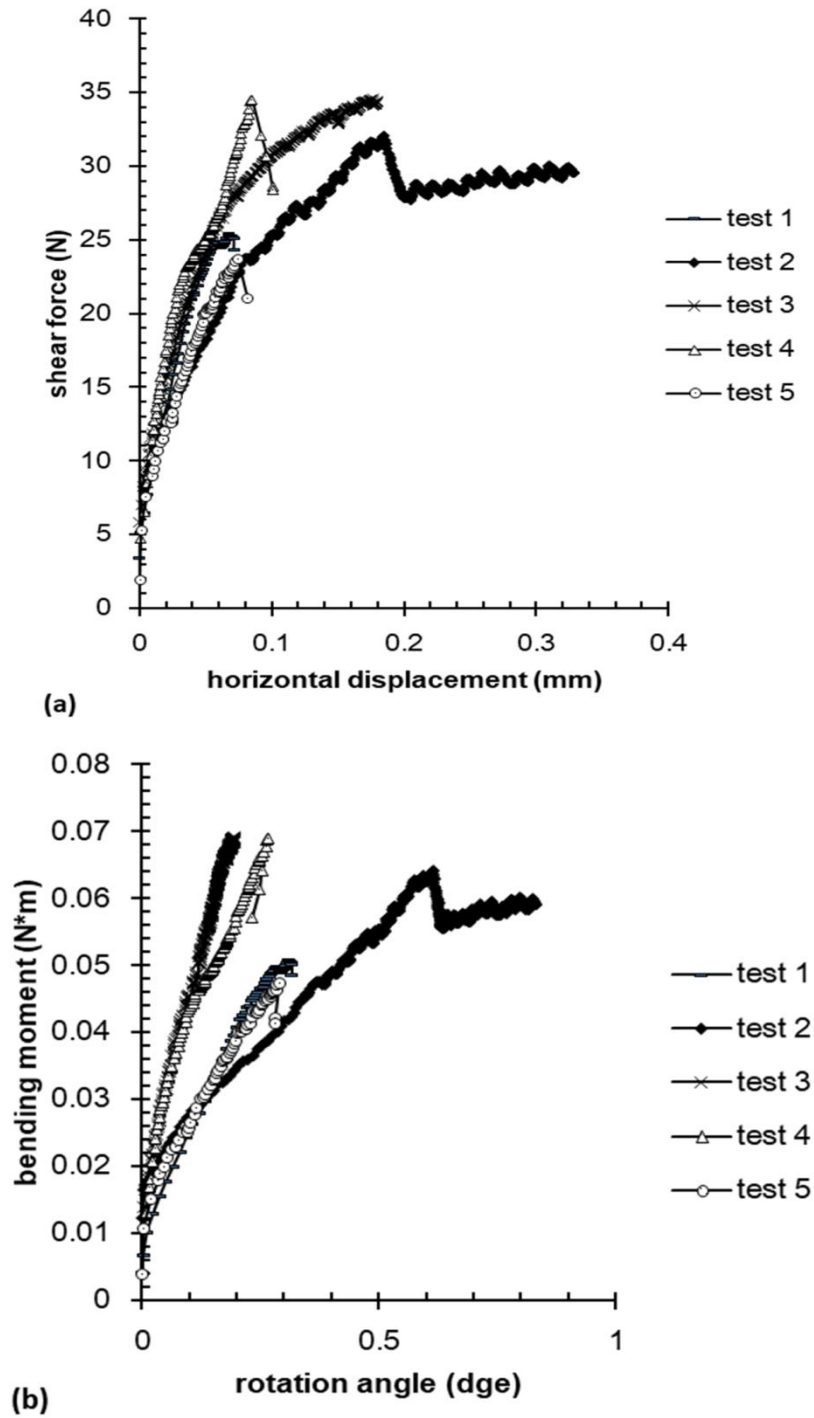


**Figure 7** Mechanical response for the bending tests on GPLBS under a normal force of 50N (a) shear force-horizontal displacement (b) bending moment-rotation angle.